

Generalized scaling of spin qubit coherence in over 12,000 host materials

Shun Kanai^{1-4,*}, F. Joseph Heremans^{5,6}, Hosung Seo⁷, Gary Wolfowicz^{5,6}, Christopher P. Anderson^{6,8}, Sean E. Sullivan⁵, Giulia Galli^{5,6,9}, David D. Awschalom^{5,6,8}, and Hideo Ohno^{1,3,4,10,11}

¹ *Laboratory for Nanoelectronics and Spintronics, Research Institute of Electrical Communication, Tohoku University, 2-1-1 Katahira, Aoba-ku, Sendai 980-8577, Japan*

² *Division for the Establishment of Frontier Sciences of Organization for Advanced Studies at Tohoku University, Tohoku University, 2-1-1 Katahira, Aoba-ku, Sendai 980-8577, Japan*

³ *Center for Science and Innovation in Spintronics, Tohoku University, 2-1-1 Katahira, Aoba-ku, Sendai 980-8577, Japan*

⁴ *Center for Spintronics Research Network, Tohoku University, 2-1-1 Katahira, Aoba-ku, Sendai 980-8577, Japan*

⁵ *Center for Molecular Engineering and Materials Science Division, Argonne National Laboratory, Lemont, IL 60439, USA*

⁶ *Pritzker School of Molecular Engineering, University of Chicago, Chicago, IL 60637, USA*

⁷ *Department of Physics and Department of Energy Systems Research, Ajou University, Suwon, Gyeonggi 16499, Republic of Korea*

⁸ *Department of Physics, University of Chicago, Chicago, IL 60637, USA*

⁹ *Department of Chemistry, University of Chicago, Chicago, IL 60637, USA*

¹⁰ *Center for Innovative Integrated Electronic Systems, Tohoku University, 468-1 Aramaki Aza Aoba, Aoba-ku, Sendai 980-0845, Japan*

¹¹ *WPI-Advanced Institute for Materials Research, Tohoku University, 2-1-1 Katahira, Aoba-ku, Sendai 980-8577, Japan*

* e-mail: skanai@tohoku.ac.jp

Spin defect centers with long quantum coherence times (T_2) are key solid-state platforms for a variety of quantum applications^{1,2}. Recently, cluster correlation expansion (CCE) techniques have emerged as a powerful tool to simulate the T_2 of defect electron spins in these solid-state systems with good accuracy³⁻⁸. Here, based on CCE, we uncover an algebraic expression for T_2 generalized for host compounds with dilute nuclear spin baths, which enables a quantitative and comprehensive materials exploration with a near instantaneous estimate of the coherence. We investigate more than 12,000 host compounds at natural isotopic abundance, and find that silicon carbide (SiC), a prominent widegap semiconductor for quantum applications^{1,2,5,8-13}, possesses the longest coherence times among widegap non-chalcogenides. In addition, more than 700 chalcogenides are shown to possess a

longer T_2 than SiC. We suggest new potential host compounds with promisingly long T_2 up to 47 ms, and pave the way to explore unprecedented functional materials for quantum applications.

Defect centers have been used to demonstrate a wide range of functionalities, including remote entanglement¹⁵, control of large nuclear spin clusters¹⁶, and quantum sensing of local temperature¹⁷, magnetic field¹⁸, electric field¹⁹, and strain²⁰. While these functionalities have been investigated in only a few solid-state systems, new defects and host materials may offer a new range of opportunities. Weber, Koehl, Varley *et al*¹ consolidated the generalized criteria of the preferable properties of the hosts for spin qubit applications²: a wide bandgap, small spin-orbit coupling, nuclear spin free lattice, and availability of high-quality single crystal. These criteria led to the identification of SiC as a promising host for qubits, which broadened the field beyond the NV⁻ center in diamond and uncovered a varied landscape of materials for defect spin qubits with different relative advantages and disadvantages.

For most quantum applications, the key property of interest is the electron spin coherence time, generally defined as T_2 by Hahn echo measurement, *i.e.* after refocusing of slow fluctuating noises by a single π -pulse¹⁰. The electron spin T_2 is limited by the interaction of the spin with its surrounding electric, thermal, and magnetic noise. However, in the absence of additional paramagnetic defects or the spin relaxation time (T_1) limitations, in most quantum applications, the electron spin T_2 is well predicted by only considering the effect of nuclear spins in the host materials, especially in high quality, wide-bandgap systems at cryogenic temperatures. For a $S = 1/2$ electron spin interacting with a few $I = 1/2$ nuclear spins, analytical solutions for the electron spin echo envelope modulation (ESEEM) have existed for half a century²¹. Yet an analytic equation is absent for efficiently predicting T_2 of a typical electron spin in a solid-state defect center interacting with several thousand nuclear spins^{3,4,7,8,22}, which is highly desirable in the wide-range search of new quantum host materials.

Cluster correlation expansion^{3,4,7}, enables accurate calculations of the T_2 of an electron spin interacting with large number of nuclear spins by dividing the spins into small subsets of interacting spin clusters as shown in Fig. 1a. In particular, the pairwise treatment of nuclear spins has been shown to provide an excellent accuracy in simulating the decoherence of spin qubits in several dilute nuclear

spin host materials: Bi dopants in silicon, the NV⁻ center in diamond, and the VV⁰ center in SiC⁶⁻⁸. CCE calculations, however, are still not an easy-to-use prediction scheme, requiring derivations from first principles calculations^{23,24} and computationally expensive simulations especially for compounds with $I > 1/2$, making its use for the high throughput search of new qubit host materials limited.

Here, we use CCE to uncover a method to not only to explore over 12,000 host materials for quantum applications and discover candidates with a long electron spin coherence time, but also to provide an easy-to-use T_2 prediction scheme. We first investigate how materials with a dilute ($< 10^{22}$ cm⁻³) nuclear spin bath comprised of one or multiple nuclear spin species can be decomposed into separate independent baths for each species. We then show that the electron spin T_2 of each individual bath is scaled by its nuclear spin g-factor value, density, and quantum number regardless of the crystalline structure of the material. This results in a single phenomenological expression for estimating any compounds' T_2 without treating the spin Hamiltonian and the time evolution of spins exactly. By calculating T_2 for every element in the periodic table and mining materials databases^{25,26}, we categorize, calculate, and predict many new candidates with a long quantum coherence time. Even though T_2 can be limited by interactions other than with the nuclear bath, our results set the fundamental materials limit for spin decoherence when all other sources are eliminated.

To begin, we benchmark our CCE calculations (Methods) on known materials. Figure 1b shows the examples of calculated Hahn-echo signal ($\mathcal{L}(t_{\text{free}})$) using CCE as a function of the free evolution duration (t_{free}) in naturally abundant 4H-SiC, diamond, Si as well as typical wide band-gap oxides. We neglect the Fermi contact terms of the hyperfine interaction given the localized electronic nature of deep-level defects and a dilute nuclear spin density in the host. We also adopt the secular approximation for the hyperfine interaction, which holds when S_z is a good quantum number in the presence of a strong B , here fixed at 5 T. Within this approximation, the Hamiltonian is reduced into bath Hamiltonians treating only the nuclear spin bath⁸, meaning the calculation is mostly agnostic to the spin defect Hamiltonian. This is crucial to allow for wide scale predictions.

T_2 is obtained by fitting the calculated $\mathcal{L}(t_{\text{free}})$ with a decay function $e^{-(t_{\text{free}}/T_2)^\eta}$, where η is a stretching exponent²⁷. The envelope of the Hahn-echo signal is critically determined by the dipole-dipole interactions between nuclear spins. Figure 1c shows the $\mathcal{L}(t_{\text{free}})$ of SiO₂ (α -quartz) with $B = 300$ mT, dividing the interactions between baths of homo-, and hetero-nuclear spins in simulation. Heteronuclear spin interactions do not contribute to decoherence in this time range, supporting that the homonuclear spin-spin interaction is the main source of the decoherence due to the decoupling of the heteronuclear spin baths. Generally, when the heteronuclear dipole-dipole interactions are much smaller than the difference of their Zeeman energies, the heteronuclear spin baths are decoupled²². We find that even in a worst-case scenario, any heteronuclear spin baths can be decoupled under achievable experimental conditions (Methods).

When heteronuclear spin baths are decoupled, one can simulate a compound's Hahn echo signal by only considering the homonuclear spin baths; $\mathcal{L}(t_{\text{free}})$ is calculated by $\prod_i \mathcal{L}_i(t_{\text{free}})$ with simulating the Hahn echo signal ($\mathcal{L}_i(t_{\text{free}})$) of isotope i , resulting in approximated T_2 of a compound by that of isotope i ($T_{2,i}$)

$$T_2 \approx \left(\sum_i T_{2,i}^{-\eta_i} \right)^{-\frac{1}{\eta'}}, \quad (1)$$

with η_i and η' assumed to be 2 in most cases (Methods).

The electron spin $T_{2,i}$ depends mainly on the spin density (n_i) of nucleus i , the crystalline structure, the nuclear spin g -factor (g_i), and the nuclear spin quantum number (I_i). We compute $T_{2,i}$ with different n_i , crystalline structure, and B . The nuclear spin density and crystalline structure dependences of $T_{2,i}$ for ¹³C is shown in Fig. 2a. For $n_{^{13}\text{C}} < 10^{22}$ cm⁻³ (cf. natural abundance in diamond: 1.9×10^{21} cm⁻³), $T_{2,^{13}\text{C}}$ is well fitted by the exponential function $a_{^{13}\text{C}} n_{^{13}\text{C}}^{-1.0}$, whose exponent -1.0 reproduces previous CCE simulations for diamond and SiC^{8,28}. Most importantly, at this density $T_{2,^{13}\text{C}}$ is *independent* of the crystal structure and is governed by interactions between

“randomly” positioned ^{13}C nucleus. As n_{spin} increases above 10^{22} cm^{-3} , the effect of anisotropy of the dipole-dipole interaction^{6,7,29} becomes relevant and T_2 deviates from the exponential dependence except for in the amorphous limit.

We can therefore scale $T_{2,i}$ as $a_i n_i^{-1.0}$, where the coefficient a_i , dependent on g_i and I_i , is derived by an exponential fit to the calculated $T_{2,i}$ vs. n_i as shown in Fig. 2a. Figure 2b then presents a_i for all stable isotopes computed by CCE and the corresponding $T_{2,i}$ at $n_i = 1.0 \times 10^{20} \text{ cm}^{-3}$ as a function of g_i . The calculated data lines up well with different series of I_i . The lines are the exponential fits $a_i = b|g_i|^\beta$. Figure 2c summarizes the intercept b vs. I_i and the exponent β vs. I_i . For spin-1/2 isotopes, α has been analytically calculated to be $-13/8 \approx -1.63$ ⁷, which is shown as a dashed line in Fig. 2c, and is in good agreement with numerically obtained $\beta = -1.64(7)$ within the error bar regardless of the I_i . We find b changes with I_i and is fitted by the exponential function $b \propto I_i^{-1.10(3)}$ as shown in the dotted line, which indicates that $T_{2,i}$ can be expressed by using $(|g_i|I_i^{0.66})^{-1.6}$. Figure 2d shows $T_{2,i}$ vs. $|g_i|I_i^{0.66}$, where all the isotopes of all the elements collapse into one line within the error bars. From fitting with an exponential, we determined the phenomenological expression of a_i for all isotopes as $a_i = c|g_i|^{-1.6}I_i^{-1.1}$ with c being an isotope independent constant $= 1.5 \times 10^{18} \text{ cm}^{-3}\text{s}$. We therefore obtain the simple expression for $T_{2,i}$ with scaling factors g_i , I_i , and n_i (in cm^{-3}) as

$$T_{2,i} = 1.5 \times 10^{18} |g_i|^{-1.6} I_i^{-1.1} n_i^{-1.0} \text{ (s).} \quad (2)$$

This expression obtained by considering CCE of all stable isotopes, combined with equation (1) enables an instantaneous estimate of the T_2 with any host materials without treating defect or bath Hamiltonians for dilute nuclear spin baths. This results in a comprehensive prediction of materials with long T_2 without the need for any CCE simulations, even for high I , or complex heteronuclear systems.

We have assumed defect centers with electron g-factor $g_e = 2$ and $S = 1/2$ above, while for S

$> 1/2$ centers, a two-level system can be assigned to a given electron spin transition, acting similarly but not equivalently to $S = 1/2$ under the secular approximation. For $S = 1$, for example, T_2 is shown to be $\sim 10\%$ longer than that with $S = 1/2$ through CCE calculations⁸. Using a generalized fictitious spin for the magnetic dipole transition $|m_S^- \rangle \leftrightarrow |m_S^+ \rangle$ and recalculating the coherence using CCE, we find an expansion of equation (2) that modifies its constant prefactor c for $S = 1/2$ to $3/2$ transitions as shown in Fig. 2e. Dashed lines are the exponential fits $c \propto g_e^\delta$, and the exponent δ is ≈ -0.39 , which is in good agreement with theoretically obtained value for $S = 1/2$ and $I = 1/2$ as $-3/8 \approx -0.38$ ⁷. This is therefore a universal coherence time holding for all transitions for electron spin centers with a dilute spinful nuclear host (Supplemental Information). This expression also hints towards further possible theoretical work that may unravel the physics behind this universal scaling.

In order to prepare for a wide-scale exploration of coherence times for host materials, we investigate the T_2 of every element in the periodic table assuming a natural abundance of isotopes, as shown in Fig. 3 taking the element density (n_{element}) of $1.0 \times 10^{23} \text{ cm}^{-3}$ (Supplemental Information). This table provides a unique lens to explore and understand the spin coherence of compounds and how to compose materials. Among the elements that compose solid compounds, only cerium has no effect on T_2 , because all stable isotopes have $I_i = 0$. In addition, there are 7 elements with longer coherence than carbon, which suggests their allotropes or compounds could yield longer coherence time than that of diamond spin centers.

Finally, we demonstrate a comprehensive prediction of T_2 based on equations (1) and (2). We utilize structural information from online databases^{25,26} to automate the process, considering 12,847 stable materials with predicted bandgaps larger than 1.0 eV. Table I shows the list of the materials with $T_2 > 10 \text{ ms}$. Here we assume materials have natural isotopic abundance. We attribute the slight deviations of the values on Table I from a full CCE calculation in Fig. 1b to the error on the exponents in equation (2), the anisotropy of dipole-dipole interaction, and that η approximated to be 2, as discussed. However, the calculated difference is small and does not hinder screening materials for

quantum coherence. We find that CeO₂ has the largest T_2 of all investigated at 47 ms, which is virtually the upper limit of T_2 for all naturally abundant compounds. Beyond choosing the elements of the host crystal and reducing the dimensionality of the host²⁸, isotopic purification of the material^{13,30,31} can further extend T_2 coherence times; however, isotopic purification of certain materials is often cost prohibitive or impossible depending on isotopic species.

Of the compounds considered, there are 27 materials with natural isotopic abundance with coherence times longer than 10 ms, all of which are composed of oxides, sulfides, and sulfates.

Fig. 4 shows the types of all 832 materials with $T_2 > 1$ ms. SiC has the longest T_2 among non-chalcogenides, and our results point to the exploration of chalcogenide materials for longer T_2 times than SiC.

We offer a simple, high-throughput method to predict coherence times for spin defects to screen possible quantum host materials. This is achieved by uncovering universal scaling behavior for spin coherence in solids that depends on the effective coherence times of a compound's constituent isotopes. While we do not fully account for geometric factors such as in 2D materials²⁸, we have demonstrated the coherence time for bulk materials depends only on the nuclear spin g-value, its spin quantum number, and density regardless of crystalline structure of the compound. The predictive power of this expression points to 27 materials with coherence time longer than 10 ms and to oxides or sulfides with Ce, Fe, Ca, and Ni as cations as promising long coherence time hosts. In combination with data mining approaches³², these results present new potential materials systems with promisingly long coherence times, and pave the way to explore unprecedented and varied functional materials for quantum applications.

Methods

Spin Hamiltonian, density matrix and its time evolution. We consider the spin Hamiltonian \mathcal{H} defined by

$$\mathcal{H} = \mathcal{H}_S + \mathcal{H}_B + \mathcal{H}_{S-B}, \quad (3)$$

where \mathcal{H}_S , \mathcal{H}_B are Hamiltonians for electron spin and nuclear spins, respectively, and \mathcal{H}_{S-B} indicates electron spin – nuclear spin interaction.^{8,29,33}

$$\mathcal{H}_S = -g_e\mu_B B S_z, \quad (4)$$

$$\mathcal{H}_B = - \sum_i g_i \mu_N B I_{z,i} + \mathcal{H}_{n-n}, \quad (5)$$

$$\begin{aligned} \mathcal{H}_{S-B} &\approx \frac{\mu_0}{4\pi} g_e \mu_B \mu_N \vec{S} \cdot \sum_i g_i \left[\frac{\vec{I}_i}{r_i^3} - \frac{3(\vec{I}_i \cdot \vec{r}_i)\vec{r}_i}{r_i^5} \right] \\ &\approx S_z \sum_i \vec{A}_i \cdot \vec{I}_i, \end{aligned} \quad (6)$$

where g_e , g_i , μ_B , μ_N , and μ_0 are the g -factor of electron, the g -factor of nuclear spin of nucleus i , Bohr magneton, nuclear magneton, and the permeability of vacuum, respectively. We set the magnetic field direction to be z direction, and electron spin quantum number to be 1/2. \vec{r}_i , r_i , B , \vec{A}_i , \vec{S} , S_z , \vec{I}_i , and $I_{z,i}$ are vectors from electron spin to the nucleus i , $|\vec{r}_i|$, the magnetic field, hyperfine field vector of nucleus i , the electron spin vector operator, z component of electron spin operator, the spin operator of nucleus i , and z component of spin operator of nucleus i , respectively. \mathcal{H}_{n-n} is the Hamiltonian of nuclear spin – nuclear spin interactions;

$$\mathcal{H}_{n-n} = \frac{\mu_0}{4\pi} \mu_N^2 \sum_{\{i,j\}} g_i g_j \left[\frac{\vec{I}_i \cdot \vec{I}_j}{r_{ij}^3} - \frac{3(\vec{I}_i \cdot \vec{r}_{ij})(\vec{I}_j \cdot \vec{r}_{ij})}{r_{ij}^5} \right], \quad (7)$$

where \vec{r}_{ij} is the vector from nucleus i to nucleus j , and $r_{ij} = |\vec{r}_{ij}|$. Two of the approximations in equation (6) are valid when (1) Fermi contact term is negligible with localized electron spin center

and dilute nuclear spin in the host, which are valid in the most of the intrinsic and extrinsic defects in, *e.g.*, SiC and diamond, and (2) two of the electron spin states $m_S = \pm 1/2$ are of order GHz, *e.g.*, when one applies, for the $g = 2$ defect, a magnetic field larger than 30 mT, which is standard measurement condition for pseudospin model, respectively.

Time evolution of the density matrix $\rho(t_{\text{free}})$ is calculated by

$$\rho(t_{\text{free}}) = \mathcal{U}(t_{\text{free}})\rho(0)\mathcal{U}^\dagger(t_{\text{free}}). \quad (8)$$

We use the standard Hahn echo propagator composed of $(\pi/2)_x$ pulse, free evolution for $t_{\text{free}}/2$, π_x pulse, and free evolution for $t_{\text{free}}/2$, as

$$\mathcal{U}(t) = \exp\left(-i\frac{\mathcal{H}}{\hbar}\frac{t_{\text{free}}}{2}\right) \exp(i\pi S_x) \exp\left(-i\frac{\mathcal{H}}{\hbar}\frac{t_{\text{free}}}{2}\right) \exp\left(i\frac{\pi}{2}S_x\right). \quad (9)$$

The initial density matrix is taken to be $\rho(0) = \rho_S(0)\otimes\rho_B(0)$ using electron spin projected density matrix $\rho_S(0)$ with z projection of spin $m_S = -1/2$ state

$$\rho_S(0) = \left|-\frac{1}{2}\right\rangle\left\langle-\frac{1}{2}\right|, \quad (10)$$

and bath projected density matrix $\rho_B(0)$

$$\rho_B(0) = \sum_J P_J |J\rangle\langle J| \quad (11)$$

with P_J being the probability of the nuclear state $|J\rangle$. Hahn echo signal $\mathcal{L}(t_{\text{free}})$ is calculated by

$$\mathcal{L}(t) = \frac{\text{Tr}[\rho(t_{\text{free}})S_+]}{\text{Tr}[\rho(0)S_+]}, \quad (12)$$

where S_+ is raising operator of electron spin²¹.

Cluster correlation expansion (CCE) calculation. Hahn echo signal $\mathcal{L}^{\text{CCE}-1}$ obtained by first-, and second-order CCE (CCE-1, and CCE-2) calculations, respectively, are defined as³

$$\mathcal{L}^{\text{CCE-1}} = \prod_i \mathcal{L}_i, \quad (13)$$

$$\mathcal{L}^{\text{CCE-2}} = \mathcal{L}^{\text{CCE-1}} \prod_{\{i,j\}} \frac{\mathcal{L}_{i,j}}{\mathcal{L}_i \mathcal{L}_j}, \quad (14)$$

where \mathcal{L}_i ($\mathcal{L}_{i,j}$) is the Hahn echo signals calculated with the central electron spin and the i -th nuclear spin (electron spin and the i -th and j -th nuclear spins). It is known that in the dilute nuclear spin bath like SiC, the effect of the three or higher body spin interaction is rare and the $\mathcal{L}(t_{\text{free}})$ converges with second-order CCE^{8,28}.

Decoupling field. The envelope of the Hahn-echo signal is critically affected by the dipole-dipole interactions between nuclear spins. The dipole-dipole interaction between heteronuclear spin is characterized by two factors: Ω and δ . Ω indicates the dipole-dipole interactions between nucleus i and j , which is given by equation (7). δ indicates the energy splitting between two levels interacting with $I_{+,i}I_{-,j} + I_{-,i}I_{+,j}$ due to the different Zeeman splitting with different nuclear spin g -factors between nucleus in addition to the dipole-dipole interaction between them with $I_{\pm,i}$ being the ladder operator of spin in nucleus i given by equation (5). When $\delta \gg \Omega$, the heteronuclear spin baths are decoupled. Considering $I_{+,i}I_{-,j} + I_{-,i}I_{+,j}$ is the main source of the decoherence⁸, we estimate decoupling field B_{dec} as

$$B_{\text{dec}} = \frac{\mu_0}{4\pi} \mu_N \frac{1}{l^3} \frac{g_i g_j}{g_i - g_j}, \quad (15)$$

with l being the distance of the nearest-neighbor nucleus i , and nucleus j , respectively (Supplemental Information). For example, B_{dec} is 0.28 mT (0.13 mT) for SiO₂ (SiC), above which the heteronuclear spin baths decouple³⁴.

Using CCE calculations, Seo *et al.*, have numerically shown that $B < 30$ mT decouples

heteronuclear spin baths assuming the difference of nuclear spin g -factor values (Δg) = 0.021 and l = 1.3 Å⁸. These Δg and l values are relatively small among the compounds. Also, in experiments, B up to 300 mT ~ 1 T is achievable with a standard yoke magnet. In equation (15), the decoupling field B_{dec} is proportional to $1/l^3\Delta g$, thus, suggesting the heteronuclear spin baths are decoupled in the most of the compounds under standard experimental conditions.

As example systems, let us consider the oxide and sulfides. The ionic radius of the O²⁻ is 0.14 nm at minimum, thus B_{dec} is estimated to be $\sim g_0^2/\Delta g \times 0.9$ mT at most by equation (15), with Δg being the difference of the g -factors between ¹⁷O and cation. For the worst case among all isotopes, Δg = 0.024 for ⁹Be gives a maximum B_{dec} ~ 5 mT. For sulfides the largest B_{dec} is given by ¹⁸⁹Os with Δg = 0.011, as ~ 3 mT.

Stretching exponent. A compound's T_2 is defined by each isotope's coherence time ($T_{2,i}$) by the condition $\sum_i (T_2/T_{2,i})^{-\eta_i} = 1$, where η_i is the stretching exponent for the $\mathcal{L}_i(t)$. We find this T_2 is well approximated by

$$T_2 \approx \left(\sum_i T_{2,i}^{-\eta_i} \right)^{-\frac{1}{\eta'}}, \quad (16)$$

with η_i and η' assuming to be 2. For an example, when $T_{2,j} = T_{2,i}/10$ ($T_{2,j} = T_{2,i}/3$), T_2 in binary compound with nucleus i and j obtained by equation (1) with $\eta_i = \eta' = 2$ deviates from the exact T_2 by 0.44% (4.0%) at the very most among the typical η_i and η_j values 2–3⁸.

Materials explorations. For T_2 prediction, we have used crystallographic information framework (CIF) files available at The Materials Project^{25,26}. From CIF files, n_i is derived and T_2 is calculated by using equations (1) and (2). Only the predicted but realistic and stable materials *i.e.*, materials with zero-energy above hull are calculated.

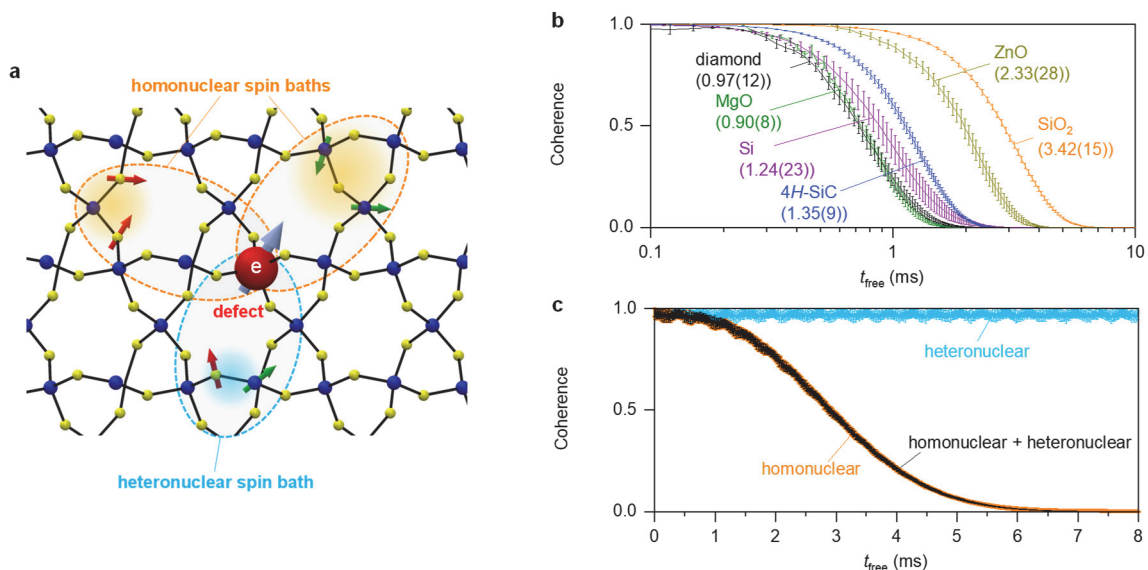


Fig. 1 | Quantum spin coherence simulation. **a**, Schematics of second-order cluster correlation expansion (CCE-2) of a defect electron spin in a heteronuclear compound. **b**, Hahn echo signal $\mathcal{L}(t_{\text{free}})$ vs. free evolution time t_{free} calculated by CCE-2 for naturally-abundant isotopic diamond, 4H-SiC, silicon, and oxides obtained by simulation under external magnetic field B of 5 T. **c**, $\mathcal{L}(t_{\text{free}})$ of SiO₂ (α -quartz) with $B = 300$ mT. In addition to the $\mathcal{L}(t_{\text{free}})$ with dipole-dipole interactions with all baths (black), that with solely homonuclear spin bath (orange), and hetero-nuclear spins (blue) are shown. Error bars indicate the sample standard deviation of the Hahn echo signal for different instances of nuclear spin coordinates.

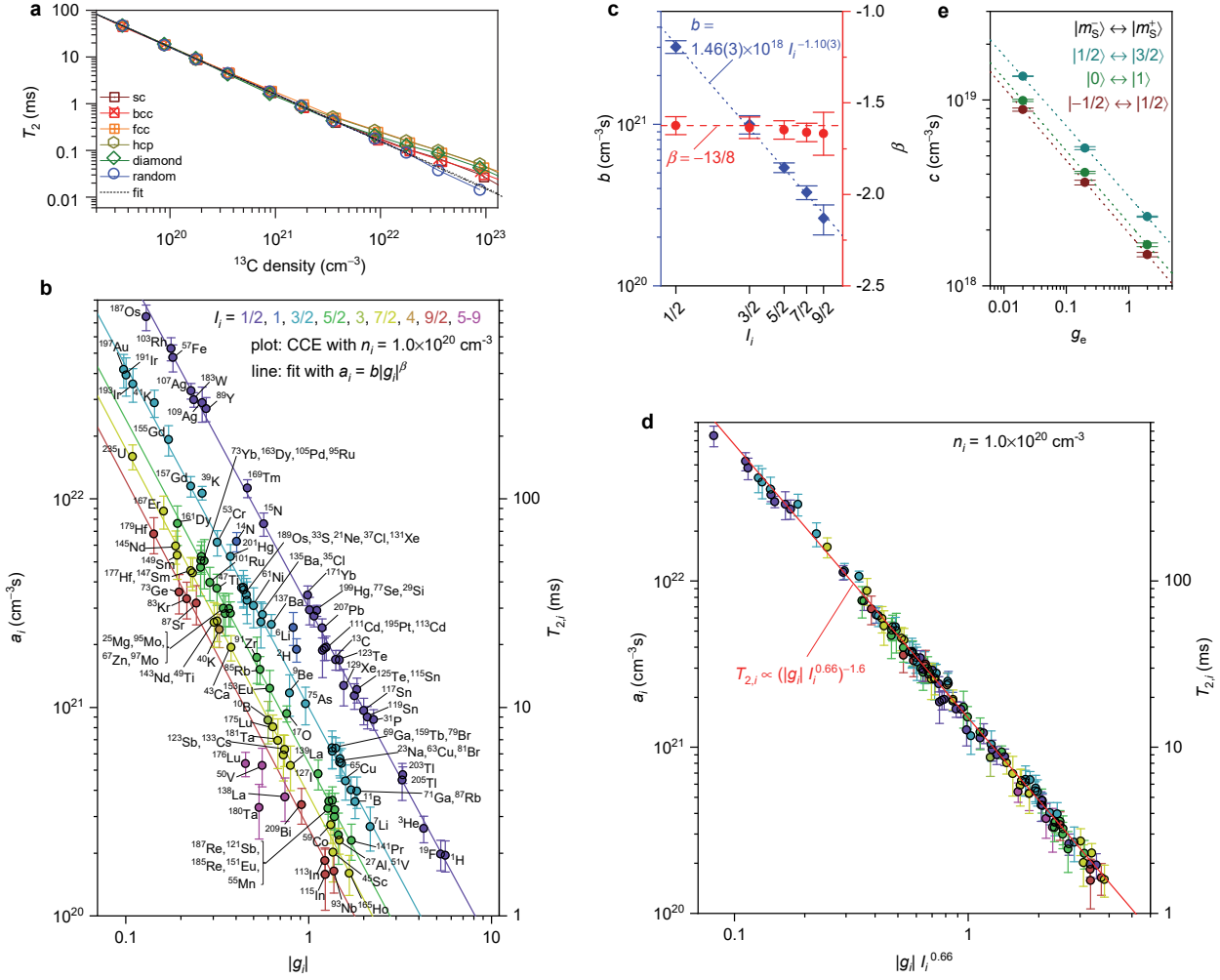


Fig. 2 | Scaling of quantum coherence of decoupled spin baths. **a**, Predicted quantum coherence time T_2 of defects in crystals composed of carbon as a function of ^{13}C density $n_i(i = {^{13}\text{C}})$ with various crystal structures. Dashed line shows the fit with an exponential function $a_i n_i^\alpha$, with a_i being coefficient, α the exponent -1.0 . An external magnetic field of 5 T is applied along [111] direction of diamond structure and along [001] directions of other crystal structures. **b**, Coefficient a_i and corresponding T_2 with nuclear spin density $n_i = 1.0 \times 10^{20} \text{ cm}^{-3}$ as a function of the absolute value of nuclear spin g_i calculated for all stable isotopes with the nuclear spin quantum number I_i . Lines are exponential fits $T_{2,i} \propto b|g_i|^\beta$ on the different half-integer- I_i spins. Error bars indicate the sample standard deviation obtained by the simulation for different crystal coordinates for the isotopes. **c**, Intercept b vs. I_i with the exponential fit $b = c I_i^{-1.10(3)}$ (blue) with c being the coefficient, and the exponent β vs. I_i with the theoretical value $\beta = -13/8$ for $I_i = 1/2$ ^{7,14} (red). **d**, T_2 vs. $|g_i| I_i^{0.66}$. Solid line is the exponential fit. All simulations are conducted under external magnetic field of 5 T . **a–d**, Electron g -factor $g_e = 2.0$ and $S = 1/2$ are assumed. **e**, Coefficient c for the transition

of electron spin states between $|m_S^-\rangle \leftrightarrow |m_S^+\rangle$ as a function of g_e . Dashed lines are the exponential fits. Error bars indicate the standard error obtained from fitting the simulated CCE data.

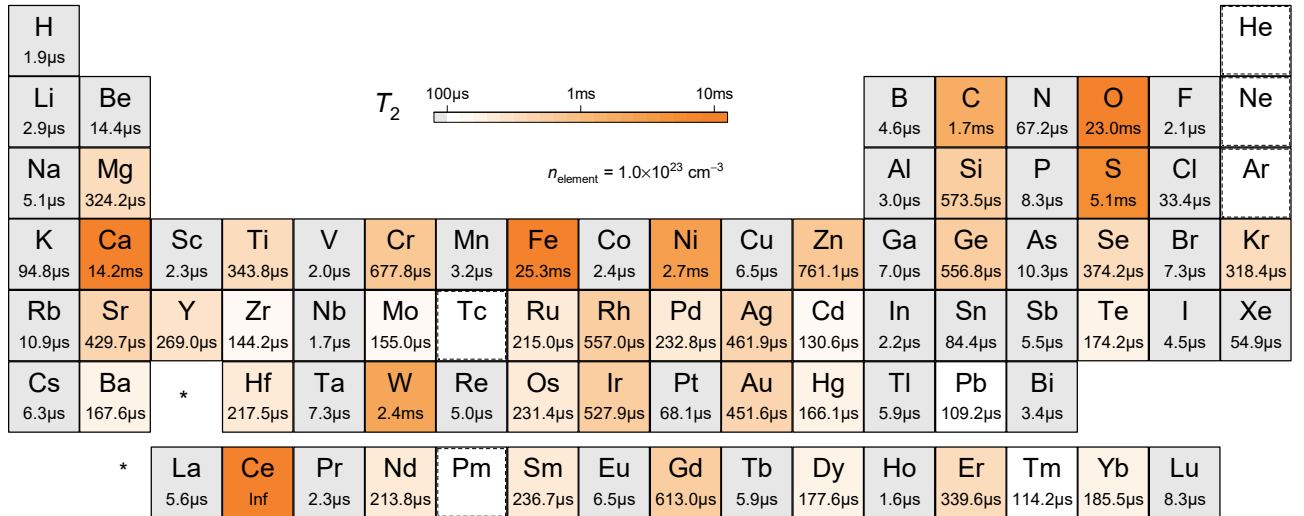


Fig. 3 | Periodic table for quantum coherence. Coherence time T_2 simulated with CCE calculations for spin qubits in hypothetical material hosts with natural abundance of a single species with element density $n_{\text{element}} = 1.0 \times 10^{23} \text{ cm}^{-3}$. The periodic table is ‘painted’ by T_2 on a log scale. Materials which are difficult to make compounds from (He, Ne, Ar) or that are without stable isotopes (Tc, Pm) are excluded.

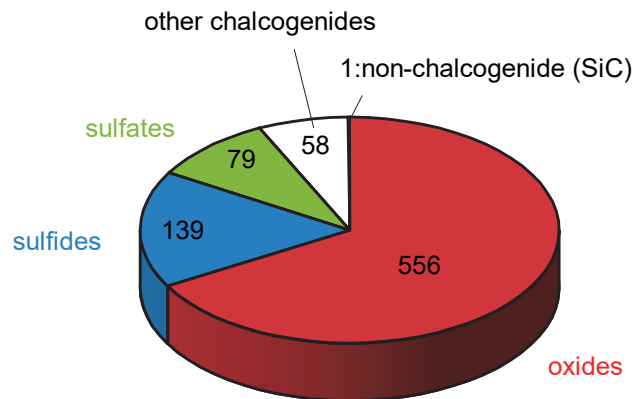


Fig. 4 | Materials to explore. Types of 832 stable compounds with quantum coherence time T_2 longer than 1 ms and bandgap larger than 1.0 eV. SiC is the only stable widegap non-chalcogenide with $T_2 > 1$ ms.

Table 1 | Top quantum coherence time T_2 materials. Materials with $T_2 > 10$ ms and bandgap > 1 eV, as well as those listed in Fig. 1b are shown.

#	Material	T_2 (ms)	#	Material	T_2 (ms)	#	Material	T_2 (ms)
1	CeO ₂	47	12	CaS	23	23	WS ₂	11
2	FeO	36	13	Ca ₂ NiWO ₆	19	24	Sr ₂ Si(S ₂ O ₇) ₄	11
3	CaO	34	14	S	19	25	Sr ₂ Ge(S ₂ O ₇) ₄	11
4	CaSO ₄	29	15	CaWO ₄	18	26	CaCO ₃	11
5	Ce(SO ₄) ₂	29	16	CS ₁₄	18	27	FeS ₂	10
6	SO ₃	29	17	Fe ₂ NiO ₄	18			
7	FeSO ₄	28	18	S ₈ O	17	138	SiO ₂	2.7
8	CaS ₃ O ₁₀	28	19	FeWO ₄	16	298	ZnO	1.9
9	Ca ₃ WO ₆	27	20	NiSO ₄	15	709	SiC	1.1
10	WS ₂ O ₉	25	21	WO ₃	13	936	diamond	0.89
11	Ca ₂ FeWO ₆	24	22	NiWO ₄	12	1125	MgO	0.60

Acknowledgements

We thank Tomasz Dietl, Fumihiro Matsukura, William A. Borders, Shunsuke Fukami, and Nikita Onizhuk for fruitful discussions, He Ma, Jaewook Lee, and Huijin Park for their help in cross-checking the CCE predictions. This work was supported in part by Marubun Research Promotion Foundation, RIEC through Overseas Training Program for Young Profession and Cooperative Research Projects, MEXT through the Program for Promoting the Enhancement of Research Universities, JSPS Kakenhi Nos. 19KK0130 and 20H02178, the EFRC Center for Novel Pathways to Quantum Coherence in Materials (NPQC) supported by DOE/BES, National Research Foundation of Korea (NRF) grant funded by the Korea government (MSIT) (No. 2018R1C1B6008980, No. 2018R1A4A1024157, and No. 2019M3E4A1078666), AFOSR FA9550-19-1-0358. Work at Argonne was supported primarily by the Center for Novel Pathways to Quantum Coherence in Materials, an Energy Frontier Research Center funded by the U.S. Department of Energy, Office of Science, Basic Energy Sciences in collaboration with the U.S. Department of Energy, Office of Science, National Quantum Information Science Research Centers.

Author contributions

D.D.A, H.O., F.J.H., and S.K. planned the study. S.K. performed CCE calculations with input from H.S., F.J.H., G.W., C.P.A., and S.E.S. All authors discussed the results and contributed to the preparation of the manuscript.

Competing interests

The authors declare no competing interests.

Data availability

The datasets generated and analyzed during the current study are available from the corresponding author upon reasonable request.

References

1. Weber, J.R., Koehl W.F., Varley J.B., Janotti A., Buckley B.B., Van de Walle C.G., Awschalom D.D. Quantum computing with defects. *Proc. Natl. Acad. Sci. U.S.A.* **107**, 8513-8518 (2010).
2. Heremans, F.J., Yale C.G., Awschalom D.D. Control of Spin Defects in Wide-Bandgap Semiconductors for Quantum Technologies. *Proc. IEEE* **104**, 2009-2023 (2016).
3. Yang, W., Liu R.B. Quantum many-body theory of qubit decoherence in a finite-size spin bath. *Phys. Rev. B* **78**, 085315 (2008).
4. Yang, W., Liu R.B. Quantum many-body theory of qubit decoherence in a finite-size spin bath. II. Ensemble dynamics. *Phys. Rev. B* **79**, 115320 (2009).
5. Onizhuk, M., Miao K.C., Blanton J.P., Ma H., Anderson C.P., Bourassa A., Awschalom D.D., Galli G. Probing the coherence of solid-state qubits at avoided crossings. Preprint at <https://arxiv.org/abs/2010.11077> (2020).
6. Balian, S.J., Wolfowicz G., Morton J.J.L., Monteiro T.S. Quantum-bath-driven decoherence of mixed spin systems. *Phys. Rev. B* **89**, 045403 (2014).
7. Hall, L.T., Cole J.H., Hollenberg L.C.L. Analytic solutions to the central-spin problem for nitrogen-vacancy centers in diamond. *Phys. Rev. B* **90**, 075201 (2014).
8. Seo, H., Falk A.L., Klimov P.V., Miao K.C., Galli G., Awschalom D.D. Quantum decoherence dynamics of divacancy spins in silicon carbide. *Nat. Commun.* **7**, 1-9 (2016).
9. Anderson, C.P., Bourassa A., Miao K.C., Wolfowicz G., Mintun P.J., Crook A.L., Abe H., Ul Hassan J., Son N.T., Ohshima T., Awschalom D.D. Electrical and optical control of single spins integrated in scalable semiconductor devices. *Science* **366**, 1225-1230 (2019).
10. Wolfowicz, G., Heremans F.J., Anderson C.P., Kanai S., Seo H., Gali A., Galli G., Awschalom D.D. Qubit guidelines for solid-state spin defects. Preprint at <https://arxiv.org/abs/2010.16395> (2020).
11. Son, N.T., Anderson C.P., Bourassa A., Miao K.C., Babin C., Widmann M., Niethammer M., Ul

- Hassan J., Morioka N., Ivanov I.G., Kaiser F., Wrachtrup J., Awschalom D.D. Developing silicon carbide for quantum spintronics. *Appl. Phys. Lett.* **116**, 190501 (2020).
12. Christle, D.J., Klimov P.V., Casas C.F.D.L., Szasz K., Ivady V., Jokubavicius V., Hassan J.U., Syvajarvi M., Koehl W.F., Ohshima T., Son N.T., Janzen E., Gali A., Awschalom D.D. Isolated Spin Qubits in SiC with a High-Fidelity Infrared Spin-to-Photon Interface. *Phys. Rev. X* **7**, 021046 (2017).
 13. Bourassa, A., Anderson C.P., Miao K.C., Onizhuk M., Ma H., Crook A.L., Abe H., Ul-Hassan J., Ohshima T., Son N.T., Galli G., Awschalom D.D. Entanglement and control of single nuclear spins in isotopically engineered silicon carbide. *Nat. Mater.* **19**, 1319-1325 (2020).
 14. Witzel, W.M., Carroll M.S., Morello A., Cywinski L., Das Sarma S. Electron spin decoherence in isotope-enriched silicon. *Phys. Rev. Lett.* **105**, 187602 (2010).
 15. Bernien, H., Hensen B., Pfaff W., Koolstra G., Blok M.S., Robledo L., Taminiau T.H., Markham M., Twitchen D.J., Childress L., Hanson R. Heralded entanglement between solid-state qubits separated by three metres. *Nature* **497**, 86-90 (2013).
 16. Bradley, C.E., Randall J., Abobeih M.H., Berrevoets R.C., Degen M.J., Bakker M.A., Markham M., Twitchen D.J., Taminiau T.H. A Ten-Qubit Solid-State Spin Register with Quantum Memory up to One Minute. *Phys. Rev. X* **9**, 031045 (2019).
 17. Fuchs, G.D., Dobrovitski V.V., Toyli D.M., Heremans F.J., Awschalom D.D. Gigahertz dynamics of a strongly driven single quantum spin. *Science* **326**, 1520-1522 (2009).
 18. Taylor, J.M., Cappellaro P., Childress L., Jiang L., Budker D., Hemmer P.R., Yacoby A., Walsworth R., Lukin M.D. High-sensitivity diamond magnetometer with nanoscale resolution. *Nat. Phys.* **4**, 810-816 (2008).
 19. Dolde, F., Fedder H., Doherty M.W., Nobauer T., Rempp F., Balasubramanian G., Wolf T., Reinhard F., Hollenberg L.C.L., Jelezko F., Wrachtrup J. Electric-field sensing using single diamond spins. *Nat. Phys.* **7**, 459-463 (2011).

20. Tamarat, P., Gaebel T., Rabeau J.R., Khan M., Greentree A.D., Wilson H., Hollenberg L.C., Prawer S., Hemmer P., Jelezko F., Wrachtrup J. Stark shift control of single optical centers in diamond. *Phys. Rev. Lett.* **97**, 083002 (2006).
21. Mims, W.B. Envelope Modulation in Spin-Echo Experiments. *Phys. Rev. B* **5**, 2409 (1972).
22. Yang, L.P., Burk C., Widmann M., Lee S.Y., Wrachtrup J., Zhao N. Electron spin decoherence in silicon carbide nuclear spin bath. *Phys. Rev. B* **90**, 241203(R) (2014).
23. Ghosh K., Ma H., Gavini V., Galli G. All-electron density functional calculations for electron and nuclear spin interactions in molecules and solids. *Phys. Rev. Mat.* **3**, 043801 (2019).
24. Ghosh K., Ma H., Onizhuk M., Gavini V., Galli G. Spin-spin interactions in solids from mixed all-electron and pseudopotential calculations – a path to screening materials for spin qubits <https://arxiv.org/abs/2102.00162> (2021).
25. Jain, A., Ong S.P., Hautier G., Chen W., Richards W.D., Dacek S., Cholia S., Gunter D., Skinner D., Ceder G., Persson K.A. Commentary: The Materials Project: A materials genome approach to accelerating materials innovation. *APL Mater.* **1**, 011002 (2013).
26. Ong, S.P., Richards W.D., Jain A., Hautier G., Kocher M., Cholia S., Gunter D., Chevrier V.L., Persson K.A., Ceder G. Python Materials Genomics (pymatgen): A robust, open-source python library for materials analysis. *Comput. Mater. Sci.* **68**, 314-319 (2013).
27. Mims, W.B. Phase Memory in Electron Spin Echoes Lattice Relaxation Effects in CaWo₄ - Er,Ce,Mn. *Phys. Rev.* **168**, 370-389 (1968).
28. Ye, M., Seo H., Galli G. Spin coherence in two-dimensional materials. *Npj Comput. Mater.* **5**, 44 (2019).
29. Zhao, N., Hu J.L., Ho S.W., Wan J.T.K., Liu R.B. Atomic-scale magnetometry of distant nuclear spin clusters via nitrogen-vacancy spin in diamond. *Nat. Nanotechnol.* **6**, 242-246 (2011).
30. Mizuuchi, N., Neumann P., Rempp F., Beck J., Jacques V., Siyushev P., Nakamura K., Twitchen D.J., Watanabe H., Yamasaki S., Jelezko F., Wrachtrup J. Coherence of single spins coupled to

- a nuclear spin bath of varying density. *Phys. Rev. B* **80**, 041201(R) (2009).
31. de Sousa, R., Das Sarma S. Theory of nuclear-induced spectral diffusion: Spin decoherence of phosphorus donors in Si and GaAs quantum dots. *Phys. Rev. B* **68**, 115322 (2003).
32. Ferrenti, A.M., de Leon N.P., Thompson J.D., Cava R.J. Identifying candidate hosts for quantum defects via data mining. *Npj Comput. Mater.* **6**, 126 (2020).
33. Maze, J.R., Dreau A., Waselowski V., Duarte H., Roch J.F., Jacques V. Free induction decay of single spins in diamond. *New. J. Phys.* **14**, 103041 (2012).
34. Zhao, N., Ho S.W., Liu R.B. Decoherence and dynamical decoupling control of nitrogen vacancy center electron spins in nuclear spin baths. *Phys. Rev. B* **85**, 115303 (2012).